https://doi.org/10.5194/acp-2019-1219
Preprint. Discussion started: 16 January 2020

Atmospheric Chemistry and Physics Discussions

Trends in global tropospheric hydroxyl radical and methane lifetime since 1850 from AerChemMIP

David S. Stevenson[1], Alcide Zhao[1], Vaishali Naik[2], Fiona M. O'Connor[3], Simone Tilmes[4], Guang Zeng[5], Lee T. Murray[6], William J. Collins[7], Paul Griffiths[8,9], Sungbo Shim[10], Larry W. Horowitz[2], Lori Sentman[2], Louisa Emmons[4]

[1]School of GeoSciences, The University of Edinburgh, EH9 3FF, United Kingdom
[2]Geophysical Fluid Dynamics Laboratory, National Oceanic and Atmospheric Administration (NOAA), Princeton, NJ08540, USA
[3]Met Office Hadley Centre, Exeter, United Kingdom
[4]Atmospheric Chemistry Observations and Modeling Laboratory, National Center for Atmospheric Research, Boulder, CO, USA
[5]National Institute of Water and Atmospheric Research, Wellington, New Zealand
[6]Department of Earth and Environmental Sciences, University of Rochester, Rochester, NY USA
[7]Department of Meteorology, University of Reading, United Kingdom
[8]National Centre for Atmospheric Science, University of Cambridge, United Kingdom
[9]Department of Chemistry, University of Cambridge, United Kingdom
[10] National Institute of Meteorological Sciences, Seogwipo-si, Jeju-do, Korea

Correspondence to: David.S.Stevenson (David.S.Stevenson@ed.ac.uk)

Abstract. We analyse historical (1850-2014) atmospheric hydroxyl (OH) and methane lifetime data from CMIP6/AerChemMIP simulations. Global OH changed little from 1850 up to around 1980, then increased by around 10%, with an associated reduction in methane lifetime. The model-derived OH trend since 1980 differs from trends found in several studies that infer OH from inversions of methyl chloroform measurements; however, these inversions are poorly constrained and contain large uncertainties that do not rule out the possibility of recent positive OH trends. The recent increases in OH that we find are consistent with one previous study that assimilated global satellite-derived carbon monoxide (CO) over the period 2002-2013. The upward trend in modelled OH since 1980 was mainly driven by changes in anthropogenic Near-Term Climate Forcer emissions (increases in anthropogenic nitrogen oxides and decreases in CO). Increases in halocarbon emissions since 1950 have made a small contribution to the increase in OH, whilst increases in aerosol-related emissions have slightly reduced OH. Halocarbon emissions have dramatically reduced the stratospheric methane lifetime, by about 15-40%, which has been assumed to not change in most previous studies. We find that whilst the main driver of atmospheric methane increases since 1850 is emissions of methane itself, increased ozone precursor emissions have significantly modulated (in general reduced) methane trends. Halocarbon and aerosol emissions are found to have relatively small contributions to methane trends. All these factors, together with changes and variations of climate and climate-driven natural emissions, need to be included in order to fully explain OH and methane trends since 1850; these factors will also be important for future trends.

1. Introduction

The hydroxyl radical (OH) is a highly reactive, and consequently very short-lived, component of the Earth's atmosphere that lies at the heart of atmospheric chemistry. It is often referred to as the cleansing agent of the atmosphere, as it is the main oxidant of many important trace gases, including methane (CH_4), carbon monoxide (CO), and non-methane volatile organic compounds (NMVOCs). Hydroxyl controls the removal rates of these

https://doi.org/10.5194/acp-2019-1219
Preprint. Discussion started: 16 January 2020

Atmospheric Chemistry and Physics Discussions

species, and hence their atmospheric residence times (e.g., Holmes et al., 2013; Turner et al., 2019). Because of this key role in determining the trace gas composition of the atmosphere, it is important to understand what controls OH's global distribution, its temporal evolution, and drivers of changes (e.g., Lawrence et al., 2001; Murray et al., 2014; Nicely et al., 2019).

The primary source of OH is from the reaction of excited oxygen atoms ($O(^1D)$) with water vapour; the excited oxygen originates from the photolysis of ozone (O_3) by ultra-violet (UV; wavelength < 330 nm) radiation:

$$O_3 + h\nu \rightarrow O_2 + O(^1D) \quad (R1)$$

$$O(^1D) + H_2O \rightarrow 2OH \quad (R2)$$

There is rapid cycling between OH and the hydroperoxyl radical (HO_2). For example, oxidation of CO and CH_4 (and other NMVOCs) consumes OH and generates HO_2:

$$CO + OH\ (+O_2) \rightarrow CO_2 + HO_2 \quad (R3)$$

$$CH_4 + OH\ (+O_2) \rightarrow CH_3O_2 + HO_2 \quad (R4)$$

Nitrogen oxides (NO and NO_2, collectively NOx) tend to push the OH/HO_2 ratio in the other direction, through the reaction:

$$NO + HO_2 \rightarrow NO_2 + OH \quad (R5)$$

However, in strongly polluted air, NO_2 becomes a sink for OH, through formation of nitric acid (HNO_3). Comprehensive descriptions of hydroxyl radical chemistry are given by, e.g., Derwent (1996), Stone et al. (2012) and Lelieveld et al. (2016).

Levels of OH are thus influenced by ambient levels of these other species – in particular, higher concentrations of CH_4, CO, and NMVOCs will reduce OH, whilst higher concentrations of NOx and H_2O will increase OH through ozone chemical production and the subsequent reaction with H_2O to produce OH, although the relative influence of different species is incompletely understood (e.g., Wild et al., 2019). As part of the Fifth Coupled Model Intercomparison Project (CMIP5), the Atmospheric Chemistry and Climate Model Intercomparison Project (ACCMIP) analysed past and future trends in OH (Naik et al., 2013; Voulgarakis et al. 2013) and attributed past changes in methane to changes in anthropogenic emissions of NOx, CH_4, CO and NMVOCs (Stevenson et al., 2013).

Direct measurement of OH is difficult (Stone et al., 2012). Trends and distributions of global OH have been derived from measurements of methyl chloroform (Krol and Lelieveld, 2003; Prinn et al., 2005; Montzka et al., 2011; Patra et al., 2014; Rigby et al., 2017), CO (Gaubert et al., 2017) and cosmogenic ^{14}CO (Krol et al., 2008). However, observationally derived global OH levels are uncertain and often show poor agreement with models. Discrepancies between measurements and models are not well understood, although new analyses of uncertainties (Naus et al., 2019) and new techniques, including Machine Learning (Nicely et al., 2019), are now being applied to the problem.

https://doi.org/10.5194/acp-2019-1219
Preprint. Discussion started: 16 January 2020

Atmospheric Chemistry and Physics Discussions

This study presents results from multiple transient 1850-2014 simulations performed for CMIP6 (Eyring et al., 2016) and the associated Aerosol and Chemistry Model Intercomparison Project (AerChemMIP; Collins et al., 2017), and is organised as follows. Section 2 describes how CMIP6 models simulated OH, and methods used for inferring OH trends from measurements. In Section 3 we present pre-industrial (PI; here taken as the 1850s) and present-day (PD) zonal mean fields of modelled OH and related species, together with historical time-series of global tropospheric OH, and corresponding CH_4 loss rates and lifetimes, including from sensitivity experiments that isolate the effects of specific emissions. Section 4 discusses the results, comparing trends in OH from measurements and models and estimates the roles of specific drivers in the historical evolution of OH. We draw conclusions in Section 5.

2. Methods

2.1 AerChemMIP CMIP6 experiments and models

We used coupled historical transient (1850-2014) model simulations from CMIP6 (Eyring et al., 2016) and various atmosphere-only historical model simulations from the associated AerChemMIP (Collins et al., 2017). Results from three global state-of-the-art Earth System Models that include detailed tropospheric and stratospheric chemistry were analysed: GFDL-ESM4, CESM2-WACCM, and UKESM1 (Table 1).

Two base historical transient experiments have been analysed: "historical" and "histSST" (Table 2). The "historical" runs included a fully coupled ocean, and multiple ensemble members. The "histSST" simulations were single member atmosphere-only runs, with monthly mean time-evolving sea-surface temperatures (SSTs) and sea-ice prescribed from one ensemble member of the historical simulations. Identical historical anthropogenic forcings were applied in all base runs by using prescribed greenhouse gas and halocarbon concentrations (Meinshausen et al., 2017) and anthropogenic and biomass burning emissions of near-term climate forcers (NTCF; i.e. aerosols and aerosol precursors, and ozone precursors) (van Marle et al., 2017; Hoesly et al., 2018). Emissions of NOx, CO and NMVOC from 1850-2014 are shown in Figure 1. Natural emissions of these species were either prescribed (e.g., soil NOx emissions, oceanic CO emissions) or internally calculated (e.g., biogenic isoprene, lightning NOx) by embedded process-based climate-dependent schemes that differ between models (e.g., Archibald et al., 2019). Methane concentrations were prescribed at the surface based on observations and ice core data (Meinshausen et al., 2017); away from the surface, methane was simulated by the model. However, by prescribing surface concentrations, methane throughout the model domain was effectively prescribed (Figure S1). We also analysed several variants of the histSST base case, with either methane concentrations or emissions of NTCFs fixed at pre-industrial levels, or halocarbon concentrations fixed at 1950 levels. These variants allow us to estimate the roles of different drivers on OH (Table 2).

For some model variables we separated fields at the tropopause (e.g., to provide a methane lifetime with respect to loss processes in the troposphere and stratosphere as separate values). We used World Meteorological Organisation (WMO) defined tropopause pressures from the models to diagnose this masking. The exact definition used is not critical, as most oxidation occurs well away from the tropopause in the tropical lower atmosphere (cf. tropospheric ozone, where the tropopause definition is much more important; Griffiths et al., submitted).

https://doi.org/10.5194/acp-2019-1219
Preprint. Discussion started: 16 January 2020

Atmospheric Chemistry and Physics Discussions

Models diagnosed methane loss rates due to chemical destruction in each grid-box – these are dominated by reaction with OH (R4), but also include other reactions, such as the reaction of methane with Cl in the stratosphere. We have used these loss rates to calculate grid-box methane lifetimes. Whole atmosphere lifetimes were calculated by dividing the total methane burden by the total loss flux over the whole model domain (or just the troposphere or stratosphere, for tropospheric and stratospheric lifetimes).

We used the histSST-piNTCF simulations to diagnose the methane-OH feedback factor (Prather, 1996). These simulations held NTCF emissions at PI levels, but methane concentrations evolved following its historical trajectory; from 1950 onwards, halocarbon concentrations also increased. The methane-OH feedback is normally diagnosed from dedicated experiments that perturb only the methane concentration, but such experiments are only available for PI conditions (e.g., Thornhill et al., submitted). The methane-OH feedback factor, f, was calculated follows:

$$f = 1/(1-(\ln(\tau_{1930\text{-}1960}/\tau_{1850})/\ln([CH_4]_{1930\text{-}1960}/[CH_4]_{1850}))) \quad (1)$$

where τ is the total methane lifetime (additionally including a soil sink; CH_4 is taken to have a lifetime with respect to soil uptake of 150 yr (Prather et al., 2012)), $[CH_4]$ is the global mean methane concentration; both for a particular year(s) of the histSST-piNTCF simulation. The reference year is 1850, the first year of the simulation. We took average values between 1930 and 1960 to give the most reliable estimate of f, as this is after a sufficiently large methane perturbation has built up, but before halocarbons interfere with the results in these simulations (see Section 3.3).

We used each model's feedback factor to calculate equilibrium PD methane concentrations ($[CH_4]_{eq}$) for each sensitivity run, using the diagnosed total methane lifetimes from these experiments. The equilibrium methane concentration is the methane concentration that would have been reached if methane concentrations had not been prescribed in these runs, but rather that methane emissions had been applied, allowing methane concentrations to evolve freely (e.g., Stevenson et al., 2013):

$$[CH_4]_{eq} = [CH_4]_{ref} (\tau_{PD}/\tau_{ref})^f \quad (2)$$

where $[CH_4]_{ref}$ is the prescribed methane concentration in the run, and τ_{ref} is the total methane lifetime in the histSST base experiment, either for PD, or, in the case of histSST-piCH4, for PI. We illustrate this with two examples: (i) in the histSST_piNTCF case, the equilibrium value is the PD methane concentration that would have been reached if all NTCF emissions been held at PI levels, whilst CH_4 emissions had followed their historical evolution; and (ii) in the histSST_piCH4 case, the equilibrium value is the PD methane concentration that would have been reached is if CH_4 emissions had been held at PI levels, but all other emissions followed their historical evolution. This allows us to clarify modelled influences on CH_4 and OH from specific emissions.

2.2 Inferred OH from measurements

Tropospheric OH has a chemical lifetime of less than a second or so, reflecting its high reactivity, making direct measurement difficult and impractical for constraining global OH distributions (e.g., Stone et al., 2012). Instead, tropospheric mean OH and its variability has traditionally been inferred from measurements of trace gases with

https://doi.org/10.5194/acp-2019-1219
Preprint. Discussion started: 16 January 2020

Atmospheric Chemistry and Physics Discussions

lifetimes longer than the timescale of tropospheric mixing and whose primary loss is via reaction with OH. If emissions are well known then observed changes in atmospheric abundance may be related, via inverse methods, to variations in OH. To date, the favoured proxy for estimating OH has been from measurements of methyl chloroform (1,1,1-trichloroethane; CH_3CCl_3; MCF), a synthetic industrial solvent that was banned in the late 1980s as a stratospheric-ozone depleting substance (Lovelock, 1977; Singh, 1977; Spivakovsky et al., 1990, 2000; Montzka et al., 2000; Prinn et al., 2001).

The earliest MCF inversions predicted relatively large OH variability, reflecting high sensitivity to the uncertainty in residual MCF emissions (Bousquet et al., 2005; Prinn et al., 2005, 2001; Krol and Lelieveld, 2003; Krol et al., 2003). However, Montzka et al. (2011) demonstrated that by the late 1990s, residual emissions had declined sufficiently so as to be a minor source of uncertainty, and that OH varied by at most a few percent in year-to-year variability. More recently, multi-box models have been used with Bayesian inverse methods to simultaneously optimize OH and MCF emissions to match MCF observations from the NOAA and the Advanced Global Atmospheric Gases Experiment (AGAGE) networks, as well as multi-species inversions including methane and methane isotopologues as additional constraints (Rigby et al., 2017; Turner et al., 2017).

The MCF inversions generally find OH to have increased from the late 1980s until the mid-2000s when OH then began to decline (top left inset of Figure 2). However, both these recent inversion studies found that optimal solutions exist within the uncertainty of the system when OH was held constant and only emissions of the reactants were allowed to be optimized. In contrast, Nicely et al. (2018) empirically derived a historic global mean OH reconstruction by taking a baseline forward OH simulation from the NASA Global Modeling Initiative (GMI) chemical-transport model driven by assimilated meteorology since 1980, and adjusting it based on box-model derived relationships of OH responses to changes in observable parameters such as total ozone columns from satellites (also shown in Figure 2). The empirically derived OH reconstruction was found to be relatively invariant when compared to the MCF inversions over the past few decades, which the study suggested reflected chemical buffering of the many competing factors that can influence OH.

Naus et al. (2019) further investigated the inversion methods used by Rigby et al. (2017) and Turner et al. (2017), confirming that the derivation of OH from MCF and CH_4 is a strongly under-constrained problem, and found that estimated OH trends with a range of different magnitudes and signs are equally valid solutions from the available data.

Gaubert et al. (2017) assimilated time-series of global-scale satellite CO measurements from the Measurement of the Pollution in the Troposphere (MOPITT) project into a global model, and found a decrease in global CO burden of ~20% over the period 2002-2013. Associated with this decrease in CO was an ~8% shortening of the methane lifetime, and a corresponding increase in OH.

3. Results

3.1 Pre-industrial to present-day base simulations

Figure 2 shows time-series (1850-2014) of global annual mean tropospheric OH burden, expressed as a percentage anomaly relative to the 1998-2007 mean value for the three models. This shows typical inter-annual variability in global OH of about ±2-3%, a small decrease (about -3%) in OH from 1850 up to 1910, then a similar magnitude increase up to the 1980s. From the 1980s to 2014, the models show a strong increase in OH of about +10%. All

https://doi.org/10.5194/acp-2019-1219
Preprint. Discussion started: 16 January 2020

Atmospheric Chemistry and Physics Discussions

three models show comparable behaviour. Figure S2 compares results between the historical and histSST runs for all models, and finds similar results between the fully coupled and the atmosphere-only experiments. This confirms that it is valid to directly compare and analyse together the results from these two experimental set-ups. Figure 2 also shows several estimates of global tropospheric OH trends over the period 1980-2014 inferred from observations (as described in Section 2.2). The published inferred trends from different inversion methods show a range of different trends, but there is little resemblance to the upwards trends simulated by the models over this time period.

Figure 3 shows present-day (PD; 2005-2014 decadal mean) zonal mean OH concentrations for the CESM2-WACCM and GFDL-AM4 models. The vertical co-ordinate is model level, and the zonal mean WMO tropopause is indicated. Both models show high OH values between 30°S and 30°N in the lower to middle troposphere, with larger values in the Northern Hemisphere (NH). Peak OH concentrations occur in the stratosphere, but it is the tropospheric OH that mainly determines the magnitude and distribution of the methane oxidation flux (Figure S3). Figure 3 also shows changes in OH from pre-industrial (PI; 1850-1859 decadal mean) to PD, expressed as the percentage change relative to PD. This reveals local increases of up to 30% in tropospheric OH, in particular over polluted regions of the NH mid-latitudes, but also a local decrease of up to 15% in the Southern Hemisphere (SH) mid- to upper troposphere at around 20°S. The PD-PI figures also show both the PD and PI tropopauses, and indicate insignificant changes in tropopause height over the historical era.

Figure 4 shows the zonal mean distribution of local methane lifetime, which ranges from about 2.5 years in the tropical lower troposphere to >20 years in colder, drier high latitudes and in the vicinity of the tropopause. Short lifetimes also occur in the stratosphere, but do not contribute significantly to the whole atmosphere lifetime due to the low air densities at high altitudes. Whole atmosphere PD (PI) lifetimes in histSST are 8.4 (9.6) yr (CESM2-WACCM), 8.3 (9.1) yr (UKESM1) and 8.6 (10.0) yr (GFDL-ESM4) (Table 3). Lifetimes have fallen since the PI, reflecting increases in OH.

3.2 Historical sensitivity simulations

The drivers of these changes in OH and methane lifetime were explored further using a range of sensitivity experiments based on the histSST simulations. These kept anthropogenic emissions or concentrations of particular species, or groups of species, at their PI or 1950 levels (Table 2). Figure 3 shows how zonal mean OH in the models responded to fixing NTCF emissions at PI levels and halocarbon concentrations at 1950 levels; Figure S5 shows additional results from the GFDL-AM4 model from the piCH4 and piO3 simulations. The panels in Figures 3 and S5 shows percentage changes in OH relative to the PD histSST base case (corresponding absolute changes in OH are shown in Figure S6). Figure 4 shows percentage changes in methane lifetime (corresponding absolute changes are shown in Figure S8). Figure 5 shows time series of how the annual tropospheric OH burden anomaly evolves in each sensitivity run, whilst Figure 6 shows the equivalent evolution of whole atmosphere methane lifetime. Figure 6 also deconvolves the methane lifetime into its tropospheric and stratospheric components.

The impact of increasing NTCF emissions was to generally increase tropospheric OH by 20-30% (Figures 3 and 5); this mainly reflects the dominant role of NOx increases, whose impact overwhelms the impacts of increasing CO (up to ~1990) and NMVOC emissions, which will have tended to reduce OH. Since about 1990, CO emissions have reduced, also contributing to the increase in OH. The overall impact of increased emissions of NTCFs has

https://doi.org/10.5194/acp-2019-1219
Preprint. Discussion started: 16 January 2020

Atmospheric Chemistry and Physics Discussions

been to reduce the methane lifetime (Figures 4 and 6, Table 3). This is mainly driven by increases in NOx emissions.

Emissions of halocarbons since 1950 have led to polar stratospheric ozone depletion, mainly in the SH. This has increased stratospheric OH levels, but also increased tropospheric OH, due to increased penetration of ultra-violet (UV) radiation, and consequently higher photolysis rates (Figure 3). The overall impact on tropospheric OH and methane lifetime is comparatively small (Figures 5 and 6, Table 3), but the impact on methane lifetime in the stratosphere has been dramatic, reducing it from ~170 yr to ~140 yr in CESM2-WACCM, and from ~140 yr to ~80 yr in GFDL-AM4 (Figure 6). These changes are mainly driven through changes in stratospheric Cl. These values can be compared to an assumed constant value for the lifetime of methane with respect to stratospheric chemical destruction of 120(±20%) yr in IPCC-AR5 (Prather et al. 2012).

Increases of methane since the PI have reduced OH (Figures 5 and S5), and lengthened the methane lifetime (Figure 6, Table 3). The effects of increased emissions of aerosols and aerosol precursors can be diagnosed by comparing the piO3 (Figure S5 and 5) and piNTCF simulations. These indicate that aerosols have slightly reduced OH and lengthened the methane lifetime, but the effect is small in magnitude compared to most other effects (Figure 6).

3.3 Contribution of OH drivers to PI-PD changes in methane

Figure 7 shows values for the methane-OH feedback factor (from a modified version Equation 1, using values for individual years, rather than 1930-1960) calculated for every year in the histSST-piNTCF simulations. In the first few decades, the methane changes are small and the variability of the methane lifetime yields large fluctuations in f. Beyond about 1960, changes in halocarbon concentrations mean that the values of f are unreliable. We therefore use the average value over the time period 1930-1960 as our best estimate of the feedback factor. This yields a value of 1.25 for CESM2-WACCM and 1.23 for GFDL-AM4. Collins et al. (submitted) find values of f from the piClim simulations of 1.34 for GFDL-AM4 and 1.35 for UKESM1. The values derived using equation (1) are probably slightly smaller because the histSST_piNTCF runs also include increases in temperature and humidity. These values are similar to the range of values found in previous studies: 1.23-1.35 (Stevenson et al., 2013; six models); 1.19-1.28 (Voulgarakis et al., 2013; two models, year 2000 conditions); and 1.33-1.45 (Prather et al., 2001; seven models). Using the values of f for 1930-1960 (Figure 7) and the lifetimes presented in Table 3, we calculate equilibrium PD methane concentrations for all sensitivity experiments (Table 4).

Observed PI and PD methane levels are 808 ppb and 1794 ppb, respectively. Holding NTCFs at PI levels increases PD methane by 16-32%. This is more intuitively interpreted in terms of the impact of the increased emissions of NTCFs: they have tended to reduce PD methane by this amount. Similarly, the impact of halocarbon emissions has been to reduce PD methane by 10-15%.

Taking results from the GFDL model alone, holding methane emissions at PI levels would have led to PD methane levels of 529 ppbv, 35% (279 ppbv) lower than PI concentrations. Hence the net impact of increasing methane emissions has been to increase methane concentrations from 529 ppbv to 1794 ppbv, an increase of 1265 ppbv. This increase is 28% larger than the simple observed PI to PD increase in methane (986 ppbv). The net impact of ozone precursor (NOx + CO + NMVOC) emissions was to reduce PD methane by 657 ppbv. Increases in halocarbon emissions reduced PD methane by 174 ppbv. Increases in aerosol-related emissions increased PD methane by 74 ppbv. These diagnosed contributions do not linearly add up to give the observed total, because a

https://doi.org/10.5194/acp-2019-1219
Preprint. Discussion started: 16 January 2020

consistent set of experiments (i.e. where all the terms are added one-by-one to a base case) has not been performed, and there are significant non-linearities in the system behaviour (i.e., the response to changes in NTCFs depends on the background levels of CH_4, etc.). This means that perfect quantitative attribution cannot be achieved. Nevertheless, the magnitudes of these terms are a useful qualitative indicator of their relative importance.

4. Discussion

The base model simulations presented here all show similar, consistent trends in global OH. They suggest relative stability of OH from the PI up to ~1980, followed by a strong (~10%) increase up to the present-day (Figures 2 and S2). The earlier stability is in good agreement with previous studies (e.g., Naik et al., 2013). The strong recent increase is at odds with several studies that use MCF and other proxies to reconstruct OH trends (e.g., Figure 2 inset); however, these show a wide range of trends. Naus et al. (2019) found that the uncertainties inherent in inversion of MCF and other proxy measures of OH are sufficiently large that OH trends derived from them are less constrained than previously thought, and that positive recent OH trends are compatible with the MCF measurements. The magnitude of the recent increase concurs with results from Gaubert et al. (2017), who assimilated satellite-derived trends in CO since 2002 into an Earth System Model.

Historical model sensitivity experiments show consistent OH responses across the models (Figure 5), and show that the evolution of methane and ozone precursor emissions have strongly influenced OH trends. Halocarbon and aerosol emissions have had relatively small impacts. These experiments did not separate the effects of different ozone precursors, but these have been explored in previous studies (Stevenson et al., 2013; Holmes et al., 2013), where increases in anthropogenic NOx emissions have been found to be the main driver of OH increases. Recent reductions in anthropogenic CO emissions (Figure 1) are clearly also important (Gaubert et al., 2017; Griffiths et al., submitted).

Although halocarbon emissions have had quite small effects on the whole atmosphere methane lifetime, they have had dramatic impacts on methane's stratospheric chemistry, where its lifetime may have reduced by up to about 40% between 1960 and 1990 (Figure 6). Previous studies generally assume a fixed stratospheric sink for methane (e.g., Prather et al, 2012).

These findings have implications for future trends in OH and methane (e.g., Holmes et al., 2013), and for how we interpret recent trends (Turner et al., 2019). The relative roles of changing emissions of methane, CO and NOx all have important competing consequences. Data assimilation of CO trends (Gaubert et al. 2017) has illustrated that this is a major driver of recent OH trends. Our results indicate that similar studies, for example assimilation of NO_2 data, may also uncover important extra information. Other studies have indicated that climate variations and change also influence OH (e.g., Murray et al., 2014; Turner et al., 2018). All these factors need to be included in holistic assessments of OH and methane change.

5. Conclusions

The CMIP6/AerChemMIP results indicate that global atmospheric OH changed little from 1850 up to around 1980, but subsequently has increased by around 10%. The model-derived trend since 1980 differs from trends found in several studies that infer OH from inversions of MCF measurements; however, these are poorly constrained and contain large uncertainties that do not rule out recent positive OH trends. The recent increases in

https://doi.org/10.5194/acp-2019-1219
Preprint. Discussion started: 16 January 2020

OH that we find are consistent with one study that assimilated global satellite-derived CO over the period 2002-2013. Further research is required to better reconcile and quantify model and measurement derived OH trends and their implications.

We find that the major drivers of the recent upward trend in OH seen in the model simulations are increases in anthropogenic NOx emissions and decreases in anthropogenic CO emissions. Increases in halocarbon emissions have made a small contribution to the increase in OH, whilst increases in aerosol-related emissions have tended to slightly reduce OH. Halocarbon emissions have dramatically reduced the stratospheric methane lifetime, by about 15-40%, and this impact should be accounted for in future studies.

The CMIP6/AerChemMIP model simulations contain many useful diagnostics that will allow us to better understand the drivers of atmospheric OH and methane trends. This study represents a very preliminary initial analysis of this rich multi-model, multi-experiment dataset.

Code and data availability

This work uses simulations from multiple models participating in the AerChemMIP project, as part of the Coupled Model Intercomparison Project (Phase 6; https://www.wcrp-climate.org/wgcm-cmip); model-specific information can be found through references listed in Table 1. Model outputs are available on the Earth System Grid Federation website (https://esgf-data.dkrz.de/search/cmip6-dkrz/). The model outputs were pre-processed using netCDF Operator (NCO) and Climate Data Operator (CDO). The analysis was carried out using Bash and Python programming languages.

Author contributions

A large team of modellers generated the data used in this study: VN, LWH and LS produced the GFDL model data; FMO, GZ, PG and SS produced the UKESM data; ST and LE produced the CESM data. AZ synthesized and analysed the data and produced the figures. DSS wrote the paper, incorporating comments from all authors.

Acknowledgements

DSS acknowledges support from the NERC grants NE/N003411/1 and NE/S009019/1, and the ARCHER UK National Supercomputing Service (http://www.archer.ac.uk). AZ acknowledges support from a Joint Scholarship from the China Scholarships Council/University of Edinburgh and the UK-China Research and Innovation Partnership Fund through the Met Office Climate Science for Service Partnership (CSSP) China as part of the Newton Fund (grant no. H5438500). GZ was supported by the NZ Government's Strategic Science Investment Fund (SSIF) through the NIWA programme CACV. WC acknowledges funding received from the European Union's Horizon 2020 research and innovation programme under grant agreement No 641816 (CRESCENDO). ST, LE and the CESM project is supported primarily by the National Science Foundation. This material is based upon work supported by the National Center for Atmospheric Research, which is a major facility sponsored by the NSF under Cooperative Agreement No. 1852977. Computing and data storage resources, including the Cheyenne supercomputer (doi:10.5065/D6RX99HX), were provided by the Computational and Information Systems Laboratory (CISL) at NCAR. SS was supported by the Korea Meteorological Administration Research

https://doi.org/10.5194/acp-2019-1219
Preprint. Discussion started: 16 January 2020

Atmospheric Chemistry and Physics Discussions

and Development Program "Development and Assessment of IPCC AR6 Climate Change Scenario", grant agreement number 1365003000.

References

Archibald, A. T., O'Connor, F. M., N. L. Abraham, S. Archer-Nicholls, M. P. Chipperfield, M. Dalvi, G. A. Folberth, F. Dennison, S. S. Dhomse, P. T. Griffiths, C. Hardacre, A. J. Hewitt, R. Hill, C. E. Johnson, J. Keeble, M. O. Köhler, O. Morgenstern, J. P. Mulcahy, C. Ordóñez, R. J. Pope, S. Rumbold, M. R. Russo, N. Savage, A. Sellar, M. Stringer, S. Turnock, O. Wild, and G. Zeng: Description and evaluation of the UKCA stratosphere-troposphere chemistry scheme (StratTrop vn 1.0) implemented in UKESM1, Geosci. Model Dev. Disc., doi.org/10.5194/gmd-2019-246, 2019.

Bousquet, P., Hauglustaine, D., Peylin, P., Carouge, C. and Ciais, P.: Two decades of OH variability as inferred by an inversion of atmospheric transport and chemistry of methyl chloroform, Atmos. Chem. Phys., 5, 2635–2656, 2005.

Collins, W. J., Lamarque, J.-F., Schulz, M., Boucher, O., Eyring, V., Hegglin, M. I., Maycock, A., Myhre, G., Prather, M., Shindell, D., and Smith, S. J.: AerChemMIP: quantifying the effects of chemistry and aerosols in CMIP6, Geosci. Model Dev., 10, 585-607, doi:10.5194/gmd-10-585-2017, 2017.

Derwent R. G.: The influence of human activities on the distribution of hydroxyl radicals in the troposphere, Philosophical Transactions of the Royal Society of London. Series A: Mathematical, Physical and Engineering Sciences, doi:10.1098/rsta.1996.0018, 1996.

Dunne, J. P., et al.: The GFDL Earth System Model version 4.1 (GFDL-ESM4.1): Model description and simulation characteristics. Journal of Advances in Modeling Earth Systems, submitted.

Emmons, L., K., Orlando, J. J., Tyndall, G., Schwantes, R. H., Kinnison, D. E., Marsh, D. R., Mills, M. J., Tilmes., S., and Lamarque, J.-F.: The MOZART Chemistry Mechanism in the Community Earth System Model version 2 (CESM2), in review, J. Adv. Modeling Earth Systems, 2019.

Eyring, V., Bony, S., Meehl, G. A., Senior, C. A., Stevens, B., Stouffer, R. J., and Taylor, K. E.: Overview of the Coupled Model Intercomparison Project Phase 6 (CMIP6) experimental design and organization, Geosci. Model Dev., 9, 1937-1958, doi:10.5194/gmd-9-1937-2016, 2016.

Gaubert, B., Worden, H.M., Arellano, A.F.J., et al.: Chemical feedback from decreasing carbon monoxide emissions. Geophysical Research Letters, 44, https://doi.org/10.1002/2017GL074987, 2017.

Gettelman, A., Mills, M. J., Kinnison, D. E., Garcia, R. R., Smith, A. K., Marsh, D. R., Tilmes, S., Vitt, F., Bardeen, C. G., McInerney, J., Liu, H.-L., Solomon, S. C., Polvani, L. M., Emmons, L. K., Lamarque, J.-F., Richter, J. H., Glanville, A. S., Bacmeister, J. T., Phillips, A. S., Neale, R. B., Simpson, I. R., DuVivier, A. K., Hodzic, A., and Randel, W. J.: The Whole Atmosphere Community Climate Model Version 6 (WACCM6), Journal of Geophysical Research: Atmospheres, p. 2019JD030943, https://doi.org/10.1029/2019JD030943, 2019.

Griffiths, P.T., Murray, L.M., Zeng, G. et al.: Tropospheric ozone in CMIP6 simulations, submitted to Atmospheric Chemistry and Physics.

Holmes, C. D., Prather, M. J., Søvde, O. A., and Myhre, G.: Future methane, hydroxyl, and their uncertainties: key climate and emission parameters for future predictions, Atmos. Chem. Phys., 13, 285–302, https://doi.org/10.5194/acp-13-285-2013, 2013

https://doi.org/10.5194/acp-2019-1219
Preprint. Discussion started: 16 January 2020

Hoesly, R. M., S. J. Smith, L. Feng, Z. Klimont, G. Janssens-Maenhout, T. Pitkanen, J. J. Seibert, L. Vu, R. J. Andres, R. M. Bolt, T. C. Bond, L. Dawidowski, N. Kholod, J. Kurokawa, M. Li, L. Liu, Z. Lu, M. C. P. Moura, P. R. O'Rourke, and Q. Zhang: Historical (1750–2014) anthropogenic emissions of reactive gases and aerosols from the Community Emissions Data System (CEDS), Geosci. Model Dev., 11, 369-408, doi.org/10.5194/gmd-11-369-2018, 2018.

Horowitz, L. W., et al., The GFDL Global Atmospheric Chemistry-Climate Model AM4.1: Model Description and Simulation Characteristics, submitted to JAMES, 2019

Krasting, J. P. et al., 2018: NOAA-GFDL GFDL-ESM4 model output prepared for CMIP6 CMIP. Version 20180701. Earth System Grid Federation. https://doi.org/10.22033/ESGF/CMIP6.1407

Krol, M., and J. Lelieveld (2003), Can the variability in tropospheric OH be deduced from measurements of 1,1,1-trichloroethane (methyl chloroform)?, J. Geophys. Res., 108(D3), 4125, doi:10.1029/2002JD002423.

Krol, M., J. Lelieveld, D. Oram, G. Sturrock, S. Penkett, C. Brenninkmeijer, V. Gros, J. Williams, and H. Scheeren (2003), Continuing emissions of methyl chloroform from Europe, Nature, 421(6919), 131–135, doi:10.1038/nature01311.

Krol, MC, et al. (2008) What can ^{14}CO measurements tell us about OH? Atmos. Chem. Phys. 8, 5033-5044

Lawrence, M. G., Jöckel, P., and von Kuhlmann, R.: What does the global mean OH concentration tell us?, Atmos. Chem. Phys., 1, 37–49, doi:10.5194/acp-1-37-2001, 2001.

Lelieveld, J., Gromov, S., Pozzer, A., and Taraborrelli, D.: Global tropospheric hydroxyl distribution, budget and reactivity, Atmos. Chem. Phys., 16, 12477–12493, https://doi.org/10.5194/acp-16-12477-2016, 2016.

Lovelock, J. E. (1977), Methyl chloroform in the troposphere as an indicator of OH radical abundance, Nature, 267(5606), 32 pp.

Meinshausen, M., E. Vogel, A. Nauels, K. Lorbacher, N. Meinshausen, D. M. Etheridge, P. J. Fraser, S. A. Montzka, P. J. Rayner, C. M. Trudinger, P. B. Krummel, U. Beyerle, J. G. Canadell, J. S. Daniel, I. G. Enting, R. M. Law, C. R. Lunder, S. O'Doherty, R. G. Prinn, S. Reimann, M. Rubino, G. J. M. Velders, M. K. Vollmer, R. H. J. Wang, and R. Weiss: Historical greenhouse gas concentrations for climate modelling (CMIP6), Geosci. Model Dev., 10, 2057-2116, doi.org/10.5194/gmd-10-2057-2017, 2017

Montzka, S., C. Spivakovsky, J. Butler, J. Elkins, L. Lock, and D. Mondeel (2000), New observational constraints for atmospheric hydroxyl on global and hemispheric scales, Science, 288(5465), 500–503.

Montzka, S. A., M. Krol, E. Dlugokencky, B. Hall, P. Joeckel, and J. Lelieveld (2011), Small interannual variability of global atmospheric hydroxyl, Science, 331(6013), 67–69, doi:10.1126/science.1197640.

Mulcahy, J. P., Johnson C., Jones C., Povey A., Sellar A., Scott C. E., Turnock S. T., Woodhouse M. T., Abraham L. N., Andrews M., Bellouin N., Browse J., Carslaw K. S., Dalvi M., Folberth G., Grosvenor D., Hardacre C., Johnson B., Jones A., Kipling Z., Mann G., Mollard J., Schutgens N., O'Connor F., Palmieri J., Reddington C., Richardson M., Stier P., Woodward S., and Yool A.: Description and evaluation of aerosol in UKESM1 and HadGEM3-GC3.1 CMIP6 historical simulations, Geosci. Model. Dev., In preparation, 2019.

Murray, L. T., Mickley, L. J., Kaplan, J. O., Sofen, E. D., Pfeiffer, M., and Alexander, B.: Factors controlling variability in the oxidative capacity of the troposphere since the Last Glacial Maximum, Atmos. Chem. Phys., 14, 3589–3622, https://doi.org/10.5194/acp-14-3589-2014, 2014.

Naik, V., Voulgarakis, A., Fiore, A. M., Horowitz, L. W., Lamarque, J.-F., Lin, M., Prather, M. J., Young, P. J., Bergmann, D., Cameron-Smith, P. J., Cionni, I., Collins, W. J., Dalsøren, S. B., Doherty, R., Eyring, V., Faluvegi,

https://doi.org/10.5194/acp-2019-1219
Preprint. Discussion started: 16 January 2020

G., Folberth, G. A., Josse, B., Lee, Y. H., MacKenzie, I. A., Nagashima, T., van Noije, T. P. C., Plummer, D. A., Righi, M., Rumbold, S. T., Skeie, R., Shindell, D. T., Stevenson, D. S., Strode, S., Sudo, K., Szopa, S., and Zeng, G.: Preindustrial to present-day changes in tropospheric hydroxyl radical and methane lifetime from the Atmospheric Chemistry and Climate Model Intercomparison Project (ACCMIP), Atmos. Chem. Phys., 13, 5277-5298, doi:10.5194/acp-13-5277-2013, 2013.

Nicely, J. M., Canty, T. P., Manyin, M., Oman, L. D., Salawitch, R. J., Steenrod, S. D., et al.: Changes in global tropospheric OH expected as a result of climate change over the last several decades. Journal of Geophysical Research: Atmospheres, 123, 10,774– 10,795. https://doi.org/10.1029/2018JD028388, 2018.

Nicely, J. M., Duncan, B. N., Hanisco, T. F., Wolfe, G. M., Salawitch, R. J., Deushi, M., Haslerud, A. S., Jöckel, P., Josse, B., Kinnison, D. E., Klekociuk, A., Manyin, M. E., Marécal, V., Morgenstern, O., Murray, L. T., Myhre, G., Oman, L. D., Pitari, G., Pozzer, A., Quaglia, I., Revell, L. E., Rozanov, E., Stenke, A., Stone, K., Strahan, S., Tilmes, S., Tost, H., Westervelt, D. M., and Zeng, G.: A Machine Learning Examination of Hydroxyl Radical Differences Among Model Simulations for CCMI-1, Atmos. Chem. Phys. Discuss., https://doi.org/10.5194/acp-2019-772, in review, 2019.

Naus, S., Montzka, S. A., Pandey, S., Basu, S., Dlugokencky, E. J., and Krol, M.: Constraints and biases in a tropospheric two-box model of OH, Atmos. Chem. Phys., 19, 407–424, https://doi.org/10.5194/acp-19-407-2019, 2019

Patra, P., Krol, M., Montzka, S. et al.: Observational evidence for interhemispheric hydroxyl-radical parity. Nature 513, 219–223, doi:10.1038/nature13721, 2014.

Prather, M.J.: Natural modes and time scales in atmospheric chemistry: theory, GWPs for CH4 and CO, and runaway growth, Geophys.Res.Lett., 23, 2597-2600, 1996.

Prather, M., D. Ehhalt, F. Dentener, R. G. Derwent, E. Dlugokencky, E. Holland, I. S. A. Isaksen, J. Katima, V. Kirchhoff, P. Matson, P. M. Midgley, and M. Wang: Chapter 4. Atmospheric Chemistry and Greenhouse Gases, in Climate Change 2001: The Scientific Basis, J.T. Houghton et al., eds., Cambridge U. Press, pp. 239-287, 2001.

Prather, M. J., Holmes, C. D., and Hsu, J.: Reactive greenhouse gas scenarios: Systematic exploration of uncertainties and the role of atmospheric chemistry, Geophys. Res. Lett., 39, L09803, doi:10.1029/2012GL051440, 2012.

Prinn, R., et al.: Evidence for substantial variations of atmospheric hydroxyl radicals in the past two decades, Science, 292(5523), 1882–1888, 2001.

Prinn, R. G., et al.: Evidence for variability of atmospheric hydroxyl radicals over the past quarter century, Geophys. Res. Lett., 32, L07809, doi:10.1029/2004GL022228, 2005.

Rigby M, et al.: Role of atmospheric oxidation in recent methane growth. Proc Natl Acad Sci USA 114:5373–5377, 2017.

Sellar, A. A., C. G. Jones,, J. Mulcahy, Y. Tang, A. Yool, A. Wiltshire, F. M. O'Connor, M. Stringer, R. Hill, J. Palmieri, S. Woodward, L. de Mora, T. Kuhlbrodt, S. Rumbold, D. I. Kelley, R. Ellis, C. E. Johnson, J. Walton, N. L. Abraham, M. B. Andrews, T. Andrews, A. T. Archibald, S. Berthou, E. Burke, E. Blockley, K. Carslaw, M. Dalvi, J. Edwards, G. A. Folberth, N. Gedney, P. T. Griffiths, A. B. Harper, M. A. Hendry, A. J. Hewitt, B. Johnson, A. Jones, C. D. Jones, J. Keeble, S. Liddicoat, O. Morgenstern, R. J. Parker, V. Predoi, E. Robertson, A. Siahaan, R. S. Smith, R. Swaminathan, M. Woodhouse, G. Zeng, and M. Zerroukat (2019): UKESM1: Description and evaluation of the UK Earth System Model, J. Adv. Modeling Earth Sys., doi.org/10.1029/2019MS001739.

https://doi.org/10.5194/acp-2019-1219
Preprint. Discussion started: 16 January 2020

Atmospheric Chemistry and Physics Discussions

Singh, H.: Preliminary estimation of average tropospheric HO concentrations in the northern and southern hemispheres, Geophys. Res. Lett., 4(10), 453–456, 1977.

Spivakovsky, C. M., R. Yevich, J. A. Logan, S. C. Wofsy, M. B. McElroy, and M. J. Prather, Tropospheric OH in a three-dimensional chemical tracer model: An assessment based on observations of CH3 CCl3 , J. Geophys. Res., 95, 18,441–18,471, 1990.

Spivakovsky, C., et al.: Three-dimensional climatological distribution of tropospheric OH: Update and evaluation, J. Geophys. Res., 105, 8931–8980, 2000.

Stevenson, D. S., Young, P. J., Naik, V., Lamarque, J.-F., Shindell, D. T., Voulgarakis, A., Skeie, R. B., Dalsoren, S. B., Myhre, G., Berntsen, T. K., Folberth, G. A., Rumbold, S. T., Collins, W. J., MacKenzie, I. A., Doherty, R. M., Zeng, G., van Noije, T. P. C., Strunk, A., Bergmann, D., Cameron-Smith, P., Plummer, D. A., Strode, S. A., Horowitz, L., Lee, Y. H., Szopa, S., Sudo, K., Nagashima, T., Josse, B., Cionni, I., Righi, M., Eyring, V., Conley, A., Bowman, K. W., Wild, O., and Archibald, A.: Tropospheric ozone changes, radiative forcing and attribution to emissions in the Atmospheric Chemistry and Climate Model Intercomparison Project (ACCMIP), Atmos. Chem. Phys., 13, 3063–3085, https://doi.org/10.5194/acp-13-3063-2013, 2013.

Stone, D., Whalley, L.K., and Heard, D.E.: Tropospheric OH and HO_2 radicals: field measurements and model comparisons, Chemical Society Reviews 41 (19), 6348-6404, 2012.

Thornhill, G.D., Collins, W.J., Kramer, R.J., Olivié, D., O'Connor, F., Abraham, N.L., Deushi, M., Emmons, L., Forster, P., Horowitz, L., Keeble, J., Lamarque, J.-F., Michou, M., Mills, M., Mulcahy, J., Myhre, G., Nabat, P., Naik, V., Oshima, N., Schulz, M., Smith, C., Takemura, T., Tilmes, S., Wu, T., Zeng, G., Zhang, J., Effective Radiative forcing from emissions of reactive gases and aerosols – a multi-model comparison, Submitted to Atmos. Chem. Phys.

Turner, A.J., C. Frankenberg, P.O. Wennberg, and D.J. Jacob: Ambiguity in the causes for decadal trends in atmospheric methane and hydroxyl, Proc. Natl. Acad. Sci., 114, 5367-5372, doi:10.1073/pnas.1616020114, 2017.

Turner, A.J., I. Fung, V. Naik, L.W. Horowitz, and R.C. Cohen: Modulation of hydroxyl variability by ENSO in the absence of external forcing, Proc. Natl. Acad. Sci., 115, 8931-8936, doi:10.1073/pnas.1807532115, 2018.

Turner, A.J., C. Frankenberg, and E.A. Kort: Interpreting contemporary trends in atmospheric methane, Proc. Natl. Acad. Sci., 116, 2805-2813, doi:10.1073/pnas.1814297116, 2019.

van Marle, M. J. E., S. Kloster, B. I. Magi, J. R. Marlon, A.-L. Daniau, R. D. Field, A. Arneth, M. Forrest, S. Hantson, N. M. Kehrwald, W. Knorr, G. Lasslop, F. Li, S. Mangeon, C. Yue, J. W. Kaiser, and G. R. van der Werf: Historic global biomass burning emissions for CMIP6 (BB4CMIP) based on merging satellite observations with proxies and fire models (1750–2015), Geosci. Model Dev., 10, 3329-3357, doi.org/10.5194/gmd-10-3329-2017, 2017.

Voulgarakis, A., Naik, V., Lamarque, J.-F., Shindell, D. T., Young, P. J., Prather, M. J., Wild, O., Field, R. D., Bergmann, D., Cameron-Smith, P., Cionni, I., Collins, W. J., Dalsøren, S. B., Doherty, R. M., Eyring, V., Faluvegi, G., Folberth, G. A., Horowitz, L. W., Josse, B., McKenzie, I. A., Nagashima, T., Plummer, D. A., Righi, M., Rumbold, S. T., Stevenson, D. S., Strode, S. A., Sudo, K., Szopa, S., and Zeng, G.: Analysis of present day and future OH and methane lifetime in the ACCMIP simulations, Atmos. Chem. Phys., 13, 2563-2587, doi:10.5194/acp-13-2563-2013, 2013.

https://doi.org/10.5194/acp-2019-1219
Preprint. Discussion started: 16 January 2020

Atmospheric Chemistry and Physics Discussions

Wild, O., Voulgarakis, A., O'Connor, F., Lamarque, J.-F., Ryan, E. M., and Lee, L.: Global sensitivity analysis of chemistry-climate model budgets of tropospheric ozone and OH: Exploring model diversity, Atmos. Chem. Phys. Discuss., https://doi.org/10.5194/acp-2019-774, in review, 2019.

503

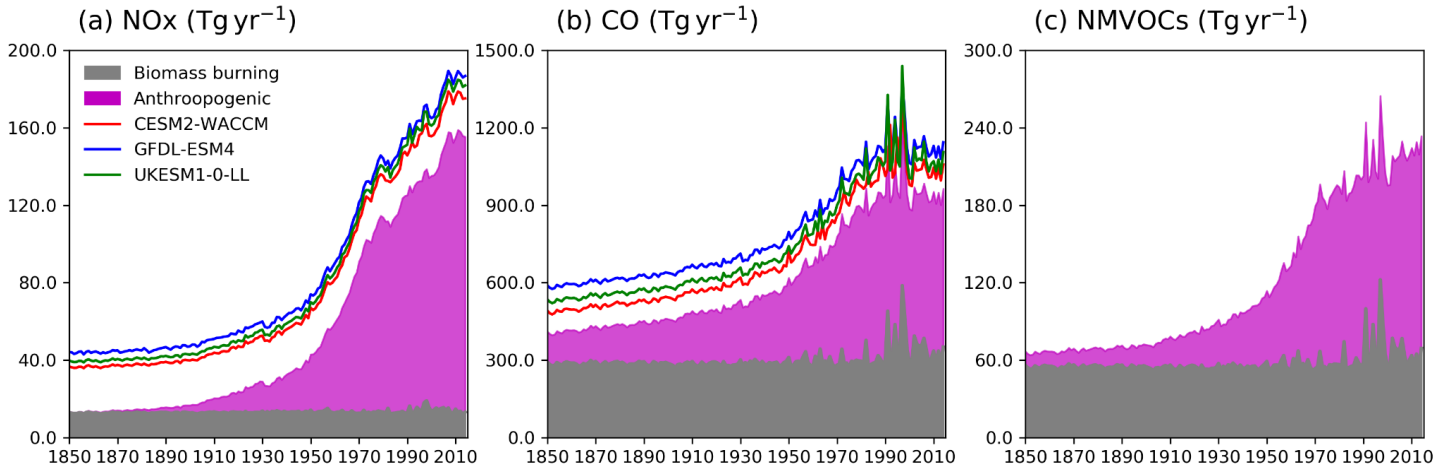

504

505 **Figure 1. Time evolution (1850-2014) of global total emission for (a) NOx (Tg(NO_2) yr^{-1}), (b) CO (Tg(CO) yr^{-1}) and (c) NMVOC (Tg(VOC) yr^{-1}). Grey for biomass burning, purple for**
506 **anthropogenic emissions. The coloured lines in the NOx and CO panels (red for CESM2-WACCM, blue for GFDL-ESM4, and green for UKESM1) are the total emission used in each**
507 **model with natural emissions included.**

508

https://doi.org/10.5194/acp-2019-1219
Preprint. Discussion started: 16 January 2020

Atmospheric Chemistry and Physics Discussions

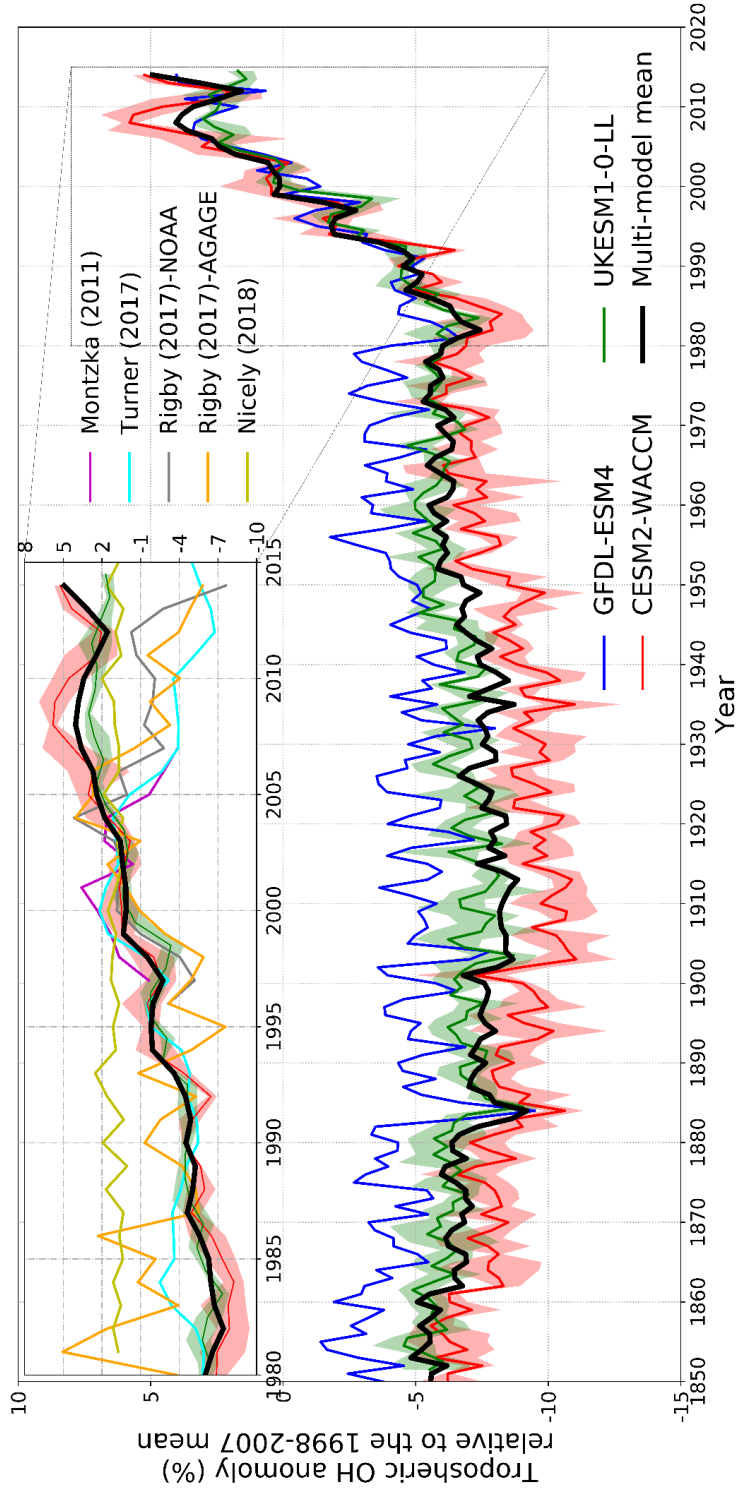

509
510 **Figure 2 Time evolution (1850-2014) of global annual mean tropospheric OH, expressed as a percentage anomaly relative to the 1998-2007 mean value for UKESM1-0LL (green),**
511 **GFDL-ESM4 (blue), and CESM2-WACCM (red). Other data in the zoomed box (1980-2015) are observation-based inversions.**
512

https://doi.org/10.5194/acp-2019-1219
Preprint. Discussion started: 16 January 2020

Atmospheric Chemistry and Physics Discussions

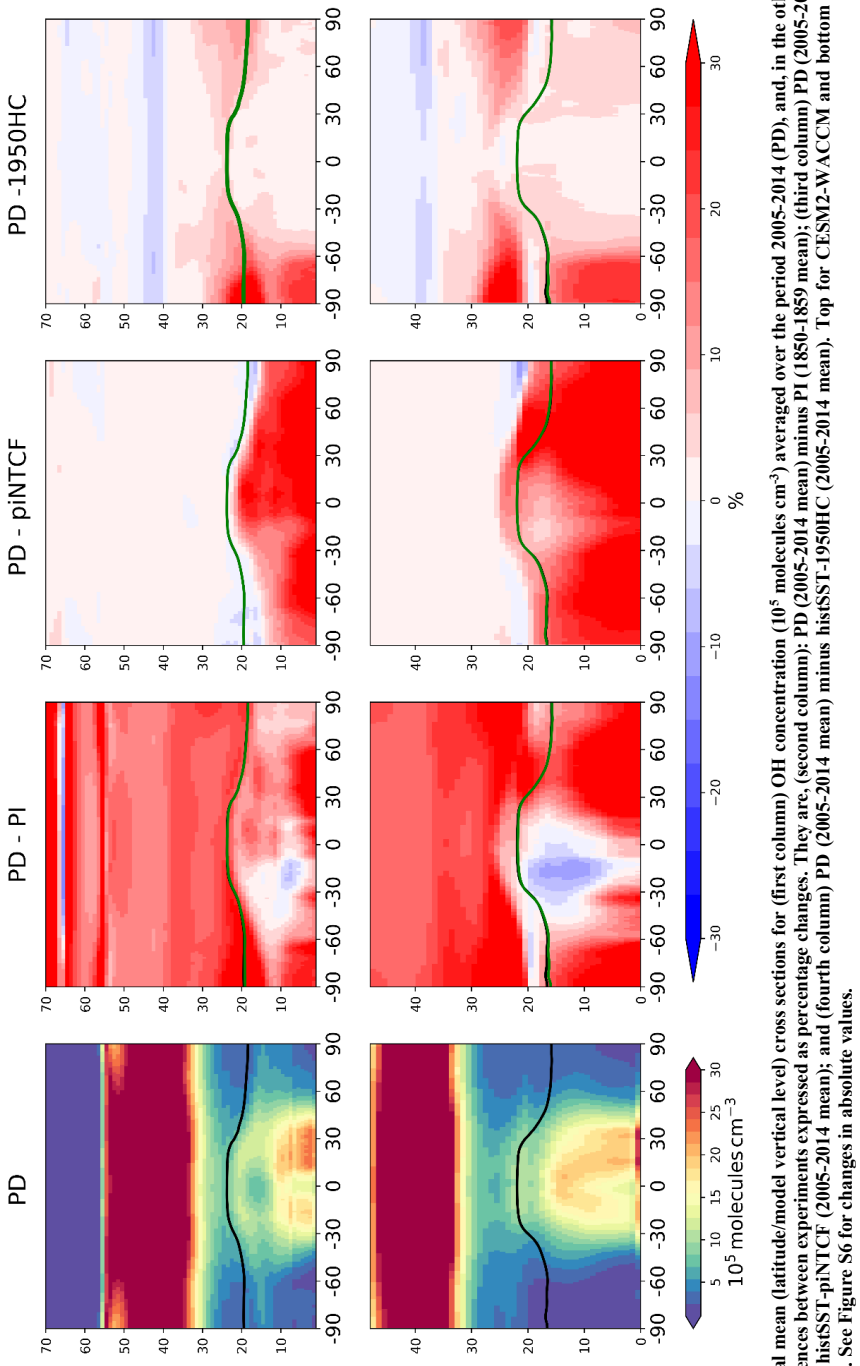

513

514 **Figure 3 Zonal mean (latitude/model vertical level) cross sections for (first column) OH concentration (10^5 molecules cm^{-3}) averaged over the period 2005-2014 (PD), and, in the other**
515 **panels, differences between experiments expressed as percentage changes. They are, (second column): PD (2005-2014 mean) minus PI (1850-1859 mean); (third column) PD (2005-2014**
516 **mean) minus histSST-piNTCF (2005-2014 mean); and (fourth column) PD (2005-2014 mean) minus histSST-1950HC (2005-2014 mean). Top for CESM2-WACCM and bottom for**
517 **GFDL-ESM4. See Figure S6 for changes in absolute values.**

https://doi.org/10.5194/acp-2019-1219
Preprint. Discussion started: 16 January 2020

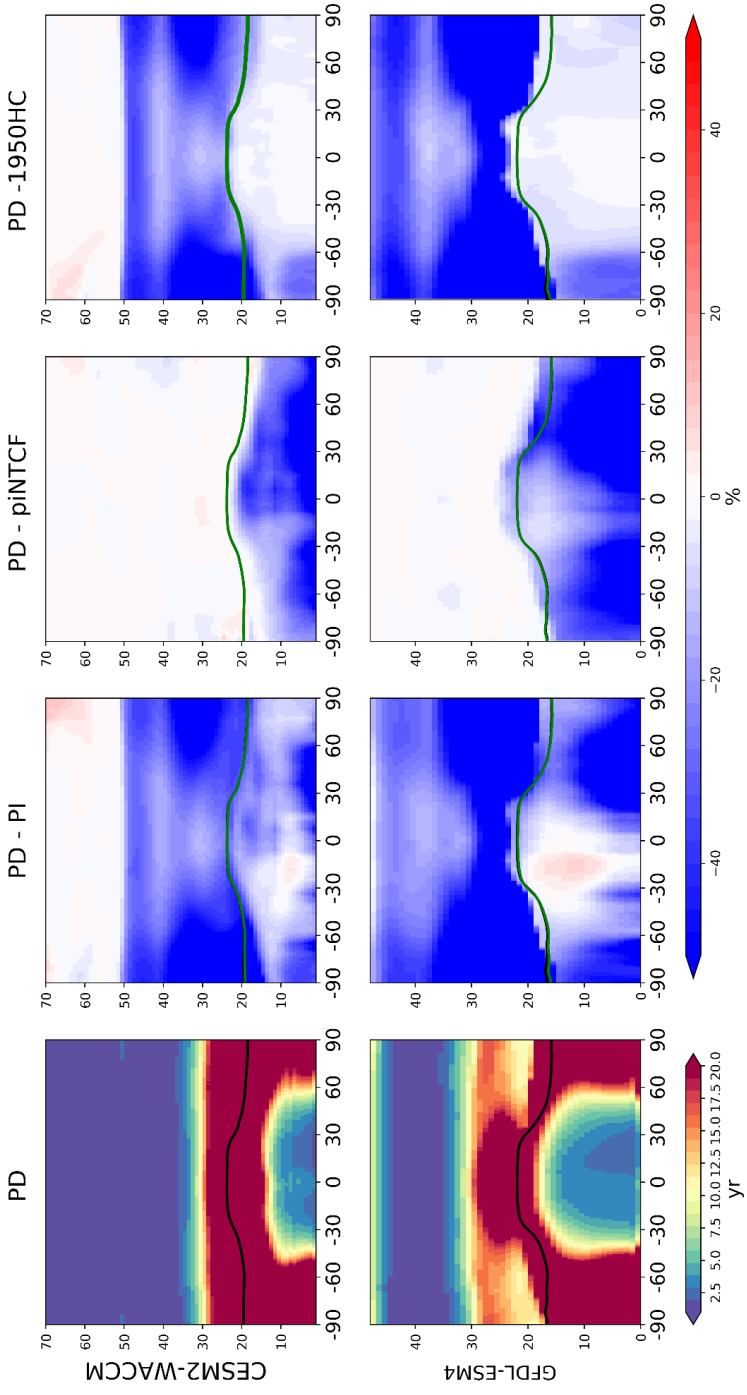

Figure 4 The same as Figure 3, but for CH_4 lifetime (yr) and the relative changes. See Figure S8 for changes in absolute values.

https://doi.org/10.5194/acp-2019-1219
Preprint. Discussion started: 16 January 2020

Atmospheric Chemistry and Physics Discussions

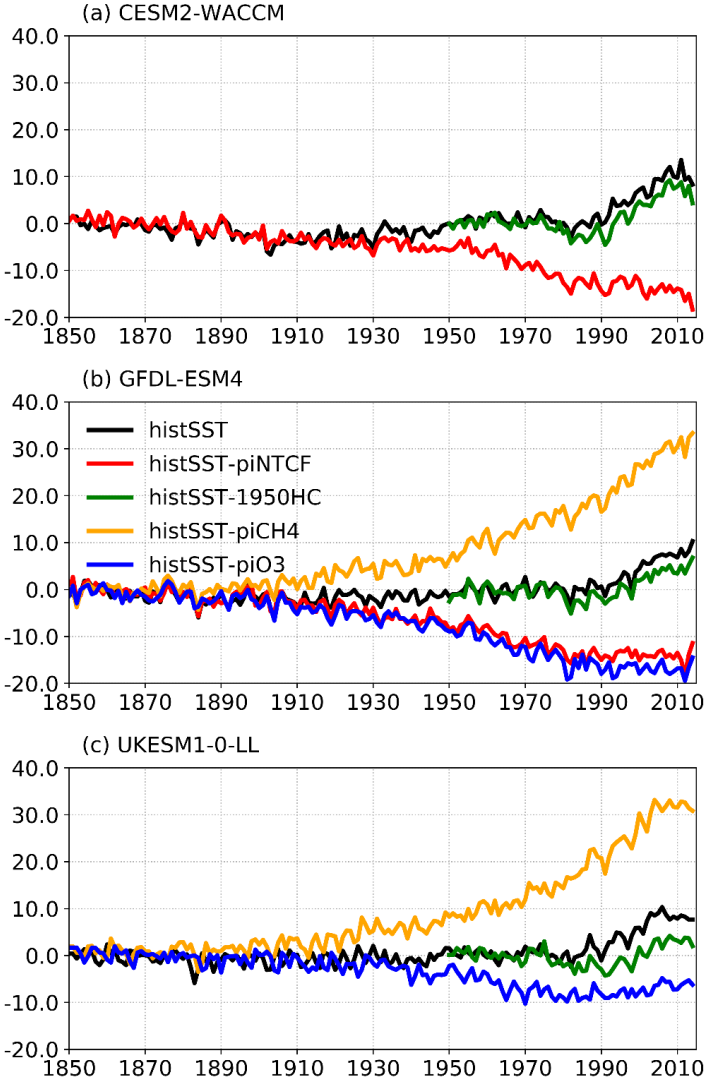

522

523 **Figure 5 Tropospheric OH anomaly (%) for sensitivity experiments from (a) CESM2-WACCM, (b) GFDL-ESM4 and**
524 **(c) UKESM1. Note the values are expressed as a percentage anomaly relative to the 1850-1859 mean value in the**
525 **histSST run in each model.**

526

https://doi.org/10.5194/acp-2019-1219
Preprint. Discussion started: 16 January 2020

Atmospheric Chemistry and Physics Discussions

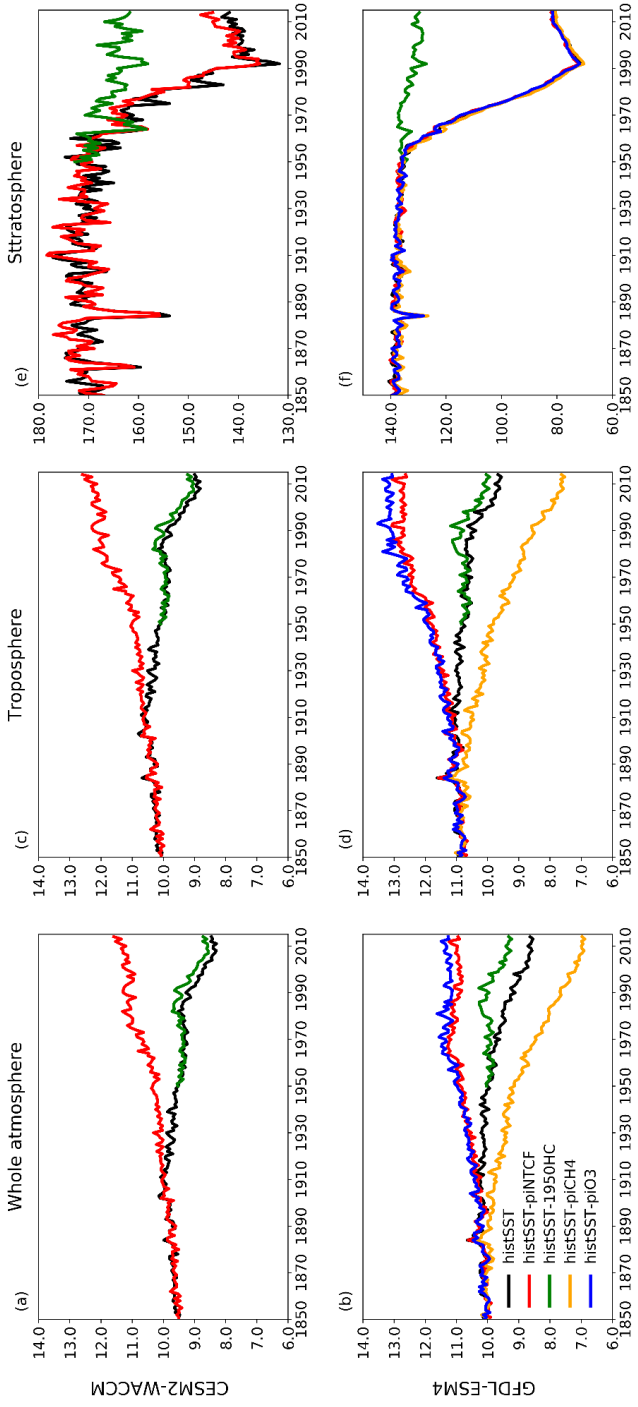

Figure 6 The same format as Figure 5, but for CH_4 lifetime (years) in the whole atmosphere (left), the troposphere (middle) and stratosphere (right).

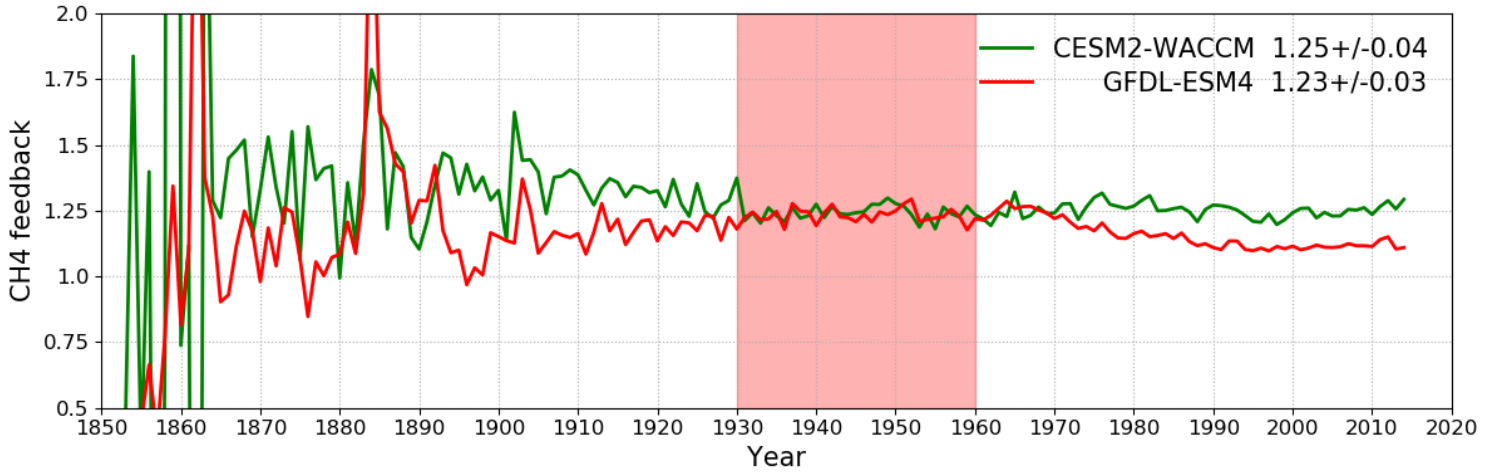

531

532

533 **Figure 7 Calculated values for the methane-OH feedback factor (f) from the histSST_piNTCF experiments for two models. Mean and Standard Deviation values for 1930-1960 (shaded)**
534 **are shown. Calculation at other times is less reliable. See text for details.**

535

https://doi.org/10.5194/acp-2019-1219
Preprint. Discussion started: 16 January 2020

Atmospheric Chemistry and Physics Discussions

Table 1: Basic details of the AerChemMIP models analysed in this study. For more details see the model references.

Model	Resolution	Chemistry scheme	Interactive emissions	Interactive deposition	Reference
CESM2 (WACCM6)	0.9° lat 1.25° long 72 levels	Detailed troposphere/ stratosphere (228 species)	BVOC using MEGAN2.1 Lightning NOx	Yes	Gettelman et al. (2019); Emmons et al. (2019)
UKESM1	1.875° long 1.25° lat 85 levels	Detailed stratosphere; 8 VOCs; 5 aerosols	BVOC Lightning NOx	Yes	Sellar et al., 2019; Archibald et al., 2019; Mulcahy et al., 2019
GFDL	C96 (cubed sphere); nominally 1° 49 levels	ATMCHEM4.1 Interactive tropospheric/ stratospheric gas-phase/ aerosol chemistry.	BVOC Lightning NOx	No	Horowitz et al. submitted; Dunne et al., submitted; Krasting et al. (2018)

https://doi.org/10.5194/acp-2019-1219
Preprint. Discussion started: 16 January 2020

Atmospheric Chemistry and Physics Discussions

Table 2: Number of ensemble members analysed from CMIP6 experiments in this study. All were transient 1850-2014 simulations, with evolving trace species emissions/GHG concentrations/land-surface. Baseline 'Historical' runs had freely evolving oceans, whilst 'histSST' runs were atmosphere only with prescribed (observed) SSTs and sea-ice. Sensitivity runs are based on histSST. The '-piNTCF' simulation held emissions of all NTCFs (aerosols and their precursors, and tropospheric ozone precursors) at PI levels. '-1950HC' held halocarbon concentrations at 1950 levels (essentially PI levels). '-piCH4' held methane concentrations at PI levels. '-piO3' held anthropogenic tropospheric ozone precursor emissions at PI levels.

	Baseline runs		Sensitivity runs (based on histSST)			
	historical	histSST	-piNTCF	-1950HC	-piCH4	-piO3
CESM2 (WACCM6)	3	1	1	1	NA	NA
UKESM1	3	1	NA	1	1	1
GFDL	1	1	1	1	1	1

https://doi.org/10.5194/acp-2019-1219
Preprint. Discussion started: 16 January 2020

Atmospheric Chemistry and Physics Discussions

555

Table 3: Whole atmosphere methane chemical (not including soil sink) lifetimes (years). PI refers to 1850-1859 mean; PD refers to 2005-2014 mean. Uncertainties are ±1 Standard Deviation, based on the range of annual values.

	Historical		HistSST		piNTCF	1950HC	piCH4	piO3
	PI	PD	PI	PD	PD	PD	PD	PD
CESM2 (WACCM 6)	9.49 ±0.06	8.19 ±0.06	9.59 ±0.07	8.40 ±0.07	9.53 ±0.07	9.46 ±0.07	NA	NA
UKESM1	8.95 ±0.07	8.08 ±0.06	9.10 ±0.08	8.26 ±0.05	NA	8.85 ±0.07	6.48 ±0.06	10.31 ±0.07
GFDL	9.86 ±0.07	8.60 ±0.07	10.03 ±0.09	8.63 ±0.05	11.01 ±0.11	9.35 ±0.07	6.97 ±0.06	11.31 ±0.09

560

https://doi.org/10.5194/acp-2019-1219
Preprint. Discussion started: 16 January 2020

Atmospheric Chemistry and Physics Discussions

565 **Table 4: Equilibrium PD global mean methane concentrations (ppbv), inferred from PD methane lifetimes from the sensitivity experiments. Also shown are percentage changes compared to the observed PD value (1794 ppbv), or for the piCH4 case, the observed PI value (808 ppbv).**

	piNTCF	1950HC	piCH4	piO3
CESM2 (WACCM6)	2082 (+16%)	2064 (+15%)	NA	NA
GFDL	2377 (+32%)	1969 (+10%)	529 (-35%)	2451 (+37%)